

Synthesis and comprehensive investigation on structural, morphological and electrical properties of PVDF-BaTiO₃ nanocomposite films

GURPREET KAUR*, DINESH SINGH RANA

Department of Instrumentation, Kurukshetra University, Kurukshetra, India

This paper presents the synthesis of polyvinylidene fluoride-barium titanate (PVDF-BaTiO₃) nanocomposite films prepared with a variable concentration of BaTiO₃ filler via solution casting technique. Here, we report the effect of BaTiO₃ over the surface morphology, crystallinity and electrical conductivity of PVDF based nanocomposite films using X-ray diffraction (XRD), Fourier transform infrared spectroscopy (FTIR), Field emission scanning electron microscopy (FESEM) and Energy dispersive spectroscopy (EDS) techniques. X-ray diffraction and FTIR studies reveal that BaTiO₃ particles are packed properly in the amorphous region of PVDF favour the alignment of dipoles of a polymer chain, which instigate the formation of β -phase. Incorporating BaTiO₃ leads to improve the crystallinity from 45.2% (for PVDF) to 59.10% (for 1 wt% of BaTiO₃). FESEM investigation showed the homogeneous dispersion of BaTiO₃ particles within the polymer matrix. Incorporating BaTiO₃ filler enhanced the electrical properties of PVDF based composite films. Observations show that the synthesized PVDF-BaTiO₃ nanocomposite films are capable to be utilized in miniaturized electronics and energy harvesting devices.

(Received November 13, 2019; accepted November 25, 2020)

Keywords: XRD, FTIR, BaTiO₃ nanoparticles, Nanocomposites, PVDF, FWHM, β -phase fraction, Crystallinity, PVDF matrix, Sol-gel

1. Introduction

Piezo-sensitive materials such as PVDF (Polyvinylidene fluoride) have gained great attention because of the ever-increasing demand for miniaturized electronics [1-5]. Due to its good piezoelectric property, PVDF is used in electromechanical sensors, electro-acoustic transducers, energy harvesting devices, and microactuators [6-10]. Because of its flexibility and chemical inertness, PVDF is used in implantable health monitoring devices [11-13]. PVDF is a long-chain polymer of alternating CH₂ and CF₂ unit, which exhibit in five different phases (α , β , γ , δ , ϵ). Out of which only β -phase shows stronger pyroelectric and piezoelectric properties because of polarization with C-F dipoles [14]. Although with good piezoelectric properties, the search for the more amenable electroactive material has moved towards the need for the development of composites that focuses to nucleate the β -phase. Doping with filler material and irradiating the polymer film and mechanical stretching of PVDF film modifies the structure of PVDF, which enhances the β -phase [2, 15-18]. Improvement in the β -phase is also affected by the solvent used and because of annealing and poling effect [19-21]. Many researchers used different filler materials for tailoring the structural and morphological properties of PVDF [2, 18]. However, no one can produce the composite film, which completely transforms multiple crystalline phases to β -phase.

In the present investigation, we have selected BaTiO₃ as filler for improving the electro-active β -phase of PVDF. BaTiO₃ has excellent dielectric properties and a high

electromechanical coupling coefficient, which makes it useful in the energy storing device [22]. BaTiO₃ is lead-free biocompatible that shows spontaneous polarization because of the displacement of Ti⁴⁺ and Ba²⁺ relative to O²⁻ ions that instigate piezoelectricity [23-24].

Herein, composite films based on PVDF incorporated with BaTiO₃ were prepared via sol-gel casting technique, to facilitate the β -phase formation, enhancement in crystallinity, and uniformity of particle distribution in the PVDF matrix. The change in morphology, crystal structure, and electrical properties of filler based PVDF films are investigated thoroughly.

2. Experimental details

2.1. Materials and synthesis

Polyvinylidene fluoride (PVDF with MW \approx 534,000) and Barium Titanate nanopowder (particle size < 100nm) used for synthesis were procured from Sigma-Aldrich, India. Dimethylformamide (DMF) used as a solvent was procured from Rankem Chemicals, India. PVDF-BaTiO₃ composite films were fabricated by the sol-gel casting method. The solution was prepared by taking 1 gram of PVDF powder and dissolved completely in 100 ml of Dimethylformamide at 50°C on a magnetic stirrer until we got a clear transparent solution. The variable concentrations of BaTiO₃ were dissolved separately in DMF under ultra-sonication for 45 mins. The variable concentrations of BaTiO₃ were calculated by the formula given below [25].

$$W(\text{wt}\%) = \frac{w_d}{(w_d + w_m)} \quad (1)$$

where w_d is the weight percentage of BaTiO_3 and w_m is the weight percentage of PVDF.

Then adding the BaTiO_3 suspension dropwise to the clear solution of PVDF and further stirring the solution for 30 mins. Before pouring the composite solution on glass slides, slides were cleaned properly by acetone and dry in the oven. Then the attained composite solution was cast over the glass slides and kept in the furnace for 10 hr at a temperature of 50°C . The composite films were gently peeled off from the slides and cut into the required dimensions for further testing.

2.2. Characterization

XRD was performed on PVDF- BaTiO_3 nanocomposite films to analyze crystal structure and phase transformation using a PANalytical X-ray diffractometer with $\text{CuK}\alpha$ radiation ($\lambda=1.54$) operated at 45 kV and 40 mA. Besides, FTIR (Perkin Elmer Frontier-ATR) was performed to analyze the change in the conformation of PVDF- BaTiO_3 nanocomposite films. The samples were analyzed in the range of $450\text{--}4000\text{ cm}^{-1}$ with an average of 20 scans. The surface morphology was observed by Field Emission Scanning Electron Microscope (Hitachi SU8010 series) with the accelerating voltage of 5000 V. The chemical composition of the composite films was analyzed by Energy Dispersive Spectroscopy. The electrical properties of PVDF- BaTiO_3 composite films were measured by studying I-V characteristics using Keithley SCS-4200.

3. Results and discussion

3.1. XRD characterization

XRD was performed to determine phases, grain size, residual stress, and crystallinity of synthesized composite films. The XRD shown in Fig. 1 represents the separate peak locations for PVDF and BaTiO_3 without the formation of any extra peak. In conformity with the work of other authors [26,27], the intense peaks observed for PVDF at 17.06° , 18.50° , 25.10° relates to α -phase whereas the peak at 20.41° belongs to β -phase. With the inclusion of BaTiO_3 , the peaks related to the α -phase of PVDF was significantly diminished with the new peaks of BaTiO_3 at 22.57° , 31.94° , 39.2° , 45.59° , 51.25° , 56.52° . The peak locations for the tetragonal phase of BaTiO_3 matches with the standard JCPDS-831880 [28-30]. As the BaTiO_3 concentration increases, the α -phase decreases with the dominance of β -phase. This is due to $\text{CH}_2\text{-CF}_2$ dipoles formulation, which was arranged in TTTT configuration, enhancing the β -phase [31,32]. This α to β phase transformation indicates the change in crystallinity (K) and

crystalline size (D) which can be calculated through Scherer relation [33].

$$D = \frac{0.9\lambda}{W \cos\theta} \quad (2)$$

Here, λ is the wavelength ($\lambda = 1.5406 \text{ \AA}$), θ is the diffraction angle and W is FWHM. FWHM and θ values can be obtained from our XRD pattern.

The crystallinity (K) was calculated from the XRD using the following relation [16, 31]:

$$K = \frac{\text{Area of crystalline peaks}}{\text{Area of (crystalline + amorphous) region}} \quad (3)$$

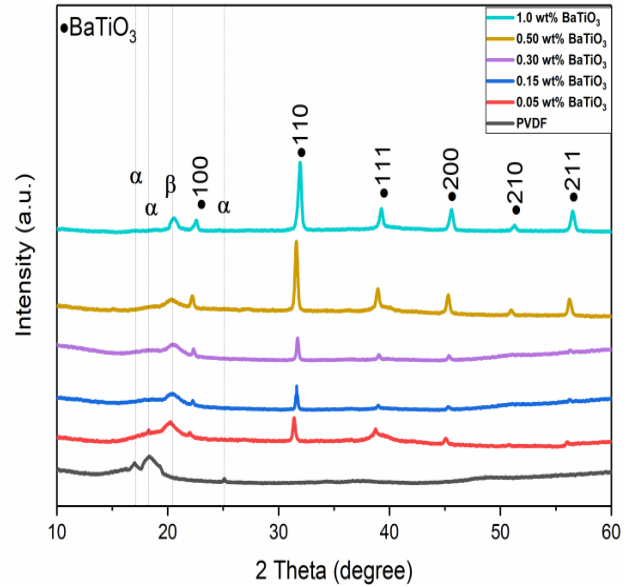


Fig. 1. X-ray diffraction of PVDF- BaTiO_3 nanocomposite films (color online)

The lattice spacing (d), dislocation density (δ) and micro-strain (ϵ) were calculated using the following relation [26, 34]:

$$\lambda = 2d \sin\theta \quad (4)$$

$$\delta = \frac{1}{D^2} \quad (5)$$

$$\epsilon = \frac{W \cos\theta}{4} \quad (6)$$

The obtained values of structural parameters for PVDF- BaTiO_3 nanocomposite films with varying concentrations of filler are tabulated in Table 1.

Table 1. The structural parameters for PVDF-BaTiO₃ nanocomposite films

BaTiO ₃ wt%	d (Å°)	D (nm)	K (%)	ε (10 ⁻³)	δ (10 ¹⁵)
0	3.81	15.38	45.23	3.55	.0133
0.05	3.17	24.86	48.42	2.39	.0091
0.15	2.85	28.19	49.80	1.97	.0052
0.30	2.77	33.17	51.71	1.81	.0050
0.50	2.69	37.03	54.02	1.41	.0035
1	2.68	40.28	59.10	1.31	.0021

From Table 1, lattice spacing (d) was found to be decreased with including BaTiO₃ particles. This may be due to the ion transfer between the PVDF and BaTiO₃. The average crystalline size (D) for the PVDF-BaTiO₃ nanocomposite films was found to be 36 nm. This increase in crystalline size is because of the agglomeration of BaTiO₃. The presence of filler and its interaction with the PVDF polymer leads to a decrease in the micro-strain (ε) and dislocation density (δ) within the PVDF matrix.

The β-phase fraction content was evaluated by comparing the intensity of peaks related to β (20.41°) and α (18.5°) phase from the XRD pattern as shown in Fig. 2 [35].

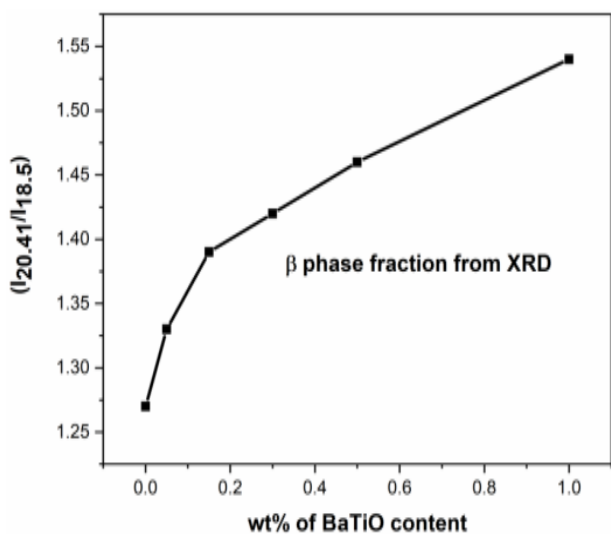


Fig. 2. The β-phase fraction content with varying concentration of BaTiO₃

In summary, it can be concluded that the inclusion of BaTiO₃ particles instigates the β-phase formation and crystallinity of PVDF based films.

3.2. FTIR Spectra analysis

FTIR spectra (shown in Fig. 3) for PVDF-BaTiO₃ films were carried out to examine the alignment of functional groups within the grid. As shown in Fig. 3, the obvious FTIR peaks at 480, 614 cm⁻¹ are due to the

bending and vibration of the CF₂ group, which demonstrated that PVDF is non-polar α-phase [35, 36]. The other peaks at 763, 874, 1070, 1168, 1232, and 1402 cm⁻¹ also attribute to α-phase [37]. The peak at 763 cm⁻¹ is due to the skeletal bending of the PVDF chain (CF-CH-CF). The peak at 874 cm⁻¹ is attributed to the rocking deformation in CH₂ and stretching in CF₂ and the peak at 1070 cm⁻¹ is attributed to rocking deformation in CH₂. The peak in 1168 and 1402 cm⁻¹ are attributed to the asymmetric stretching mode in CF₂ and scissoring deformation in CH₂ respectively. The FTIR peaks attributed to β-phase have been determined at 509, 834, and 1275 cm⁻¹ [37, 38]. The peak at 509 cm⁻¹ is attributed to CF₂ bending mode. The peak at 834 cm⁻¹ is attributed to CH₂ rocking and CF₂ asymmetric, stretching deformation; which is parallel to the chain axis. FTIR spectra for PVDF-BaTiO₃ nanocomposite films show similar absorption bands as compared to PVDF, except for the change in the intensity of peaks. This shows that composite formation does not induce any change in the atomistic bonds within the polymer structure. The inclusion of filler dominates the β-phase at absorption band 509 and 834 cm⁻¹ with the decrease in intensity of existing α-peaks at absorption band 480, 614, and 763 cm⁻¹. The phase transition is because of the interaction between Ti ions (from BaTiO₃) and F ions (from PVDF). The interfacial interaction between the negatively charged surface of BaTiO₃ and the positively charged surface of the CH₂ group, which instigates the β-phase.

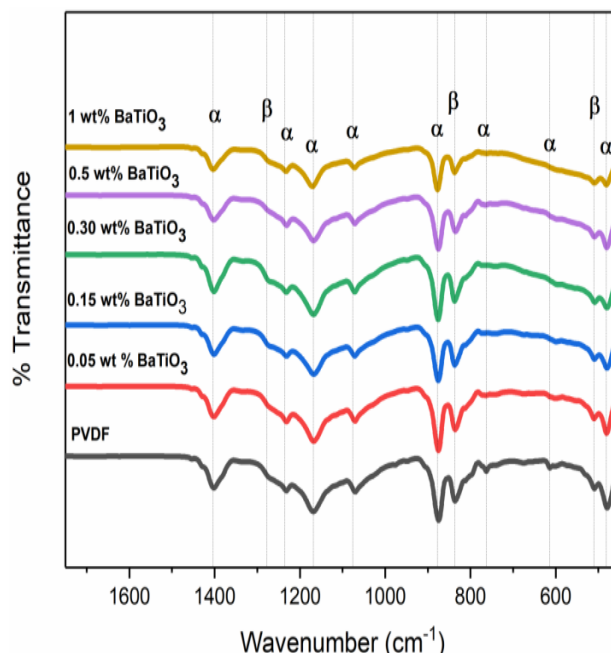


Fig. 3. FTIR spectra for PVDF-BaTiO₃ nanocomposite films (color online)

The absorbance bands at 763 cm⁻¹ and 834 cm⁻¹ relate to α-phase and β-phase respectively have been used to estimate the electro-active β-phase content by using the following formula [39].

$$F(\beta) = \frac{A_{\beta}}{1.26A_{\alpha} + A_{\beta}} = \frac{A_{\beta}}{(K_{\beta}/K_{\alpha})A_{\alpha} + A_{\beta}} \quad (7)$$

where K_{α} ($6.1 \times 10^4 \text{ cm}^2/\text{mol}$) and K_{β} ($7.7 \times 10^4 \text{ cm}^2/\text{mol}$) are the absorption coefficients of α and β phase, respectively. The variation of β -phase fraction content with an increasing concentration of BaTiO_3 has been represented in Fig. 4. The maximum rise in the β -phase fraction content is up to 0.75 (1 wt% of BaTiO_3) which is 29.38% more than PVDF. This β -phase nucleation occurs because of the stabilization of the PVDF polymer chain in trans-trans configuration. The above conclusion is in line with the results concluded from the XRD investigation.

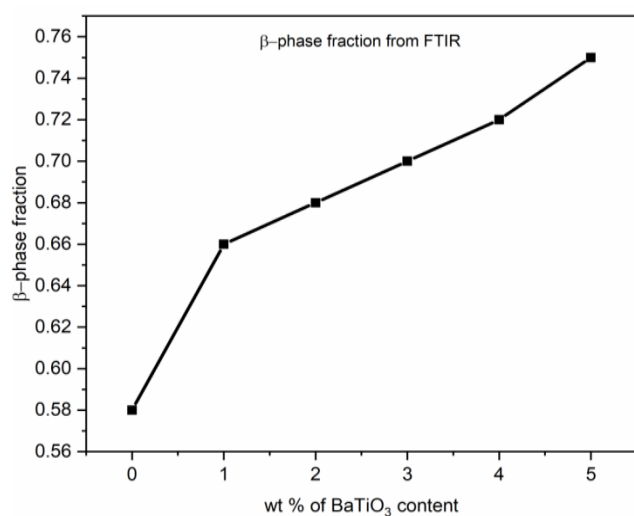


Fig. 4. The β -phase fraction content with varying concentration of BaTiO_3

3.3. FESEM analysis

Fig. 5 shows the morphological images of PVDF- BaTiO_3 nanocomposite films with varying concentrations of fillers. From the images, it can be observed that PVDF possesses a long fibre chain-like structure with the small microporous regions as analyzed by the other authors [15, 26]. On the addition of BaTiO_3 , the surface morphology of PVDF films changes with the homogeneous dispersion of filler. Because of the high density of BaTiO_3 , the particles agglomerates at the bottom to form large clusters as shown in images. The sample shows granular microstructure with micro-cracks, implying the effective interaction with filler particles and matrix. Micro-cracks observed over the surface area are because of the evaporation of the DMF during the drying process of thin films. The above results show a good agreement with XRD and FTIR.

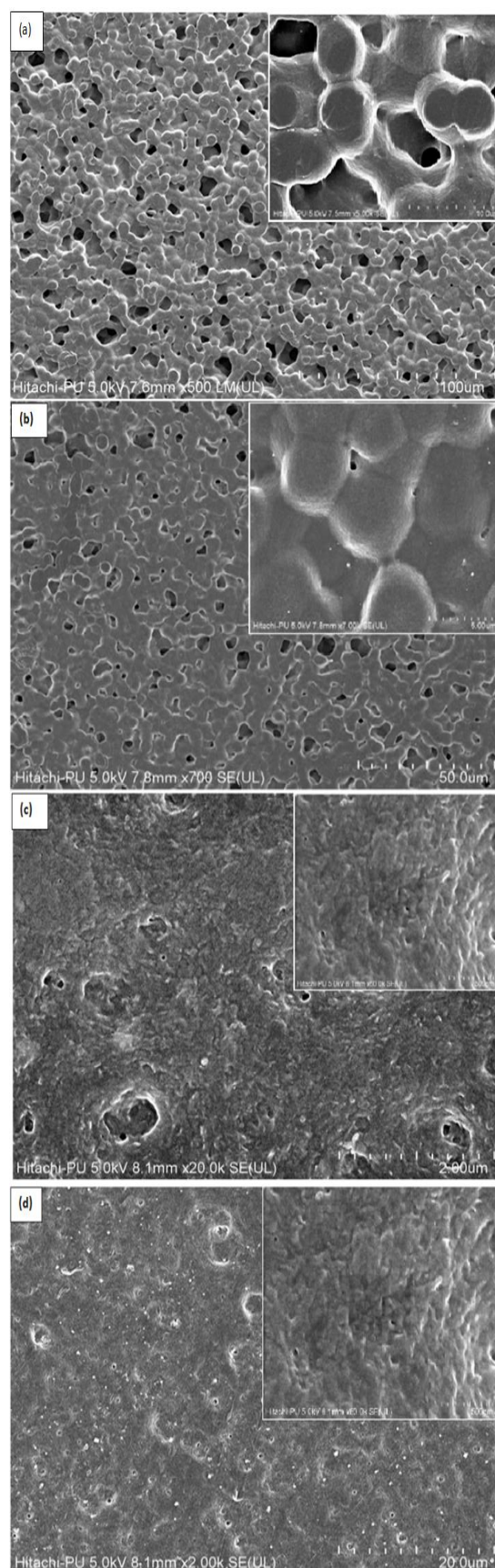


Fig. 5. FESEM images of (a) PVDF films, (b) 0.15 wt % BaTiO_3 films, (c) 0.5 wt % BaTiO_3 films, (d) 1 wt % BaTiO_3 films

3.4. Energy Dispersive Spectroscopy (EDS)

EDS is an indispensable tool for the identification of the chemical composition of composite thin films. The intensity of EDS peaks shows the fraction of different elements distributed in the sample. The elemental composition for the PVDF-BaTiO₃ nanocomposite films is shown in Fig. 6. For the PVDF, EDX spectra represent two peaks related to chemical elements, fluorine, and carbon. As the EDS cannot identify the elements with an atomic weight < 4, therefore, we cannot find hydrogen (H)

in the EDS spectra. Similarly, the EDS for PVDF-BaTiO₃ nanocomposite films show five peaks relates to chemical elements carbon (C), fluorine (F), barium (Ba), titanium (Ti), and oxygen (O). On the addition of BaTiO₃ nanoparticles, there is no such appearance of any new peak in the EDS. This reveals that there is no formation of any new intermediate chemically distinct compound on adding BaTiO₃. The intensity of elements peaks corresponding to barium (Ba), titanium (Ti), and oxygen (O) increases with the increase in the concentration of BaTiO₃ content.

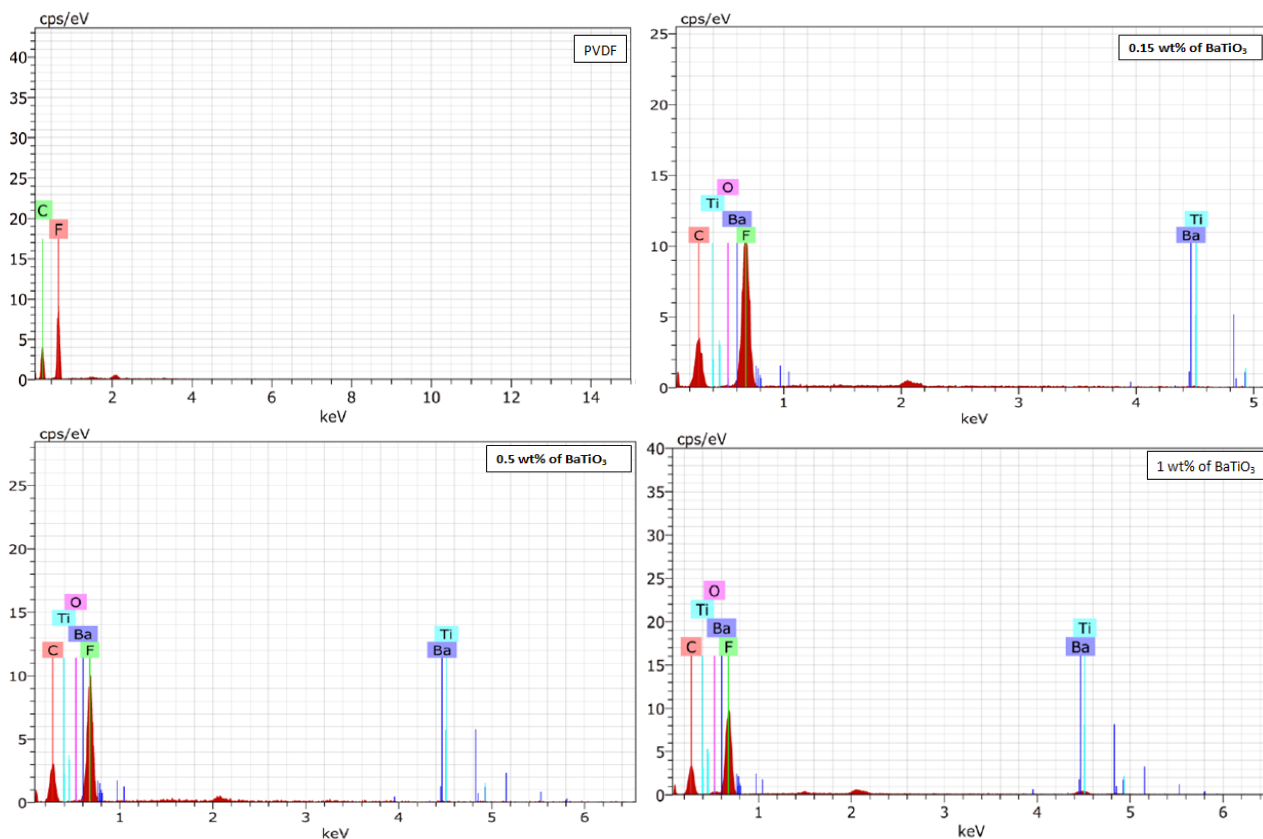


Fig. 6. EDS for (a) PVDF films, (b) 0.15 wt % BaTiO₃ films, (c) 0.5 wt % BaTiO₃ films, (d) 1 wt % BaTiO₃ films (color online)

3.5. Electrical properties

The electrical properties of PVDF-BaTiO₃ nanocomposite films with varying concentrations of filler have been investigated by I-V measurements as shown in Fig. 7. I-V measurements of PVDF samples show an almost negligible amount of current for a wide range of applied voltage. This small current with the applied voltage values arises because of the presence of free charge carriers within the PVDF grid. The introduction of BaTiO₃ nanoparticles influences the space charge regions of PVDF, resulting in an increase of current value as compare to PVDF. The rise in the current is because of the displacement of Ti⁴⁺ and Ba²⁺ relative to O²⁻ ions; orients the dipoles, which create the polarization in the direction of the field.

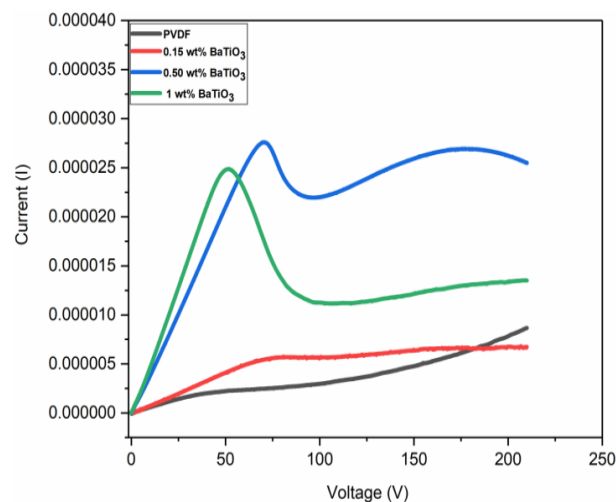


Fig. 7. I-V characteristics of PVDF- BaTiO₃ nanocomposite films (color online)

4. Conclusions

In this study, PVDF-BaTiO₃ nanocomposite films have been synthesized via a simple sol-gel casting method. XRD results reveal that BaTiO₃ particles favour the alignment of dipoles of the polymer chain, which improves the β -phase formation and crystallinity. As a result, the crystallinity enhances from 45.2% (for PVDF) to 59.10%. FTIR investigation shows that there is no major change in the characteristic band of PVDF except for an increase in the formation of β -phase. FESEM images reveal that BaTiO₃ particles were homogeneously distributed within the polymer matrix. The orientation of dipoles favours the enhancement in the electrical conductivity of PVDF-BaTiO₃ composite films because of the displacement of Ti⁴⁺ and Ba²⁺ relative to O²⁻ ions. Finally, based on results, it can be concluded that the fabricated electroactive PVDF-BaTiO₃ nanocomposite films favour the development of energy storage/harvesting devices and sensors.

Acknowledgments

We are grateful to UGC, Government of India, for financial assistance.

References

- [1] S. Khan, S. Tinku, L. Lorenzelli, R. S. Dahiya, *IEEE Sens. J.* **15**, 3146 (2015).
- [2] Anshu Mli Gaur, Dinesh Singh Rana, *J. Mater. Sci. Mater. Electronics* **27**, 2293 (2016).
- [3] D. S. Rana, D. K. Chaturvedi, J. K. Quamara, *Optoelectron. Adv. Mat.* **3**, 1354 (2009).
- [4] D. S. Rana, D. K. Chaturvedi, J. K. Quamara, *Optoelectron. Adv. Mat.* **6**, 642 (2012).
- [5] W. Chang, C. Chu, Y. Lin, *IEEE Sens.* **8**, 495 (2008).
- [6] Anshu Mli Gaur, Dinesh Singh Rana, *L. American J. of Solids and Structure* **11**, 2483 (2014).
- [7] K. Pramod, R. Gangineni, *Org. Electron.* **42**, 47 (2017).
- [8] Dudem, Bhaskar, Kim, Dong Hyun, Bharat, *J. Applied Energy Elsevier* **230**, 865 (2018).
- [9] Abolhasania, Shirvanimoghaddamb, Naebe, *J. Compos. Sci. Technol.* **138**, 49 (2017).
- [10] D. S. Rana, D. K. Chaturvedi, J. K. Quamara, *Optoelectron. Adv. Mat.* **4**, 838 (2010).
- [11] Y. Jiang, H. Hamada, S. Shiono, *Procedia Engineering* **5**, 1466 (2010).
- [12] Y. Ai, Z. Lou, S. Chen, *J. Nano Energy* **35**, 121 (2017).
- [13] D. H. Wang, S. L. Huang, *Journal of Intelligent Material Sys. and Structures* **11**, 482 (2000).
- [14] D. S. Rana, D. K. Chaturvedi, J. K. Quamara, *Optoelectron. Adv. Mat.* **3**, 737 (2009).
- [15] D. S. Rana, D. K. Chaturvedi, J. K. Quamara, *Optoelectron. Adv. Mat.* **11**, 705 (2009).
- [16] D. Mandal, K. H. Henkel, D. Schreiber, *Mater. Lett.* **73**, 123 (2012).
- [17] Elashmawi, Gaabour, Raman, *Results in Physics* **5**, 105 (2015).
- [18] Anshu Mli Gaur, Dinesh Singh Rana, *J. Material Sci. Material in Electronics* **26**, 1246 (2015).
- [19] Y. Sui, W. Chen, J. Ma, R. Hu, D. Liu, *J. RSC Adv.* **6**, 7364 (2016).
- [20] Y. K. A. Low, L. Y. Tan, L. P. Tan, *J. Appl. Polym. Sci.* **128**, 2902 (2013).
- [21] Shobhneek Kaur, A. L. Kumar, D. P. Singh, *J. Material Sci.* **28**, 8391 (2017).
- [22] M. F. Lin, P. S. Lee, *J. Mater. Chem. A* **1**, 14455 (2013).
- [23] Lee, S. J. Park, S. Kim, *Solid State Ionics Elsevier* **234**, 19 (2013).
- [24] S. F. Mendes, C. M. Costa, C. Caparros, *J. Mater. Sci.* **47**, 1378 (2012).
- [25] Anshu Mli Gaur, Dinesh Singh Rana, *J. Inorganic and Organometallic Poly. and Mater.* **29**, 1637 (2019).
- [26] D. S. Rana, D. K. Chaturvedi, J. K. Quamara, *J. Mater. Eng. Perform.* **20**, 276 (2011).
- [27] Gurpreet Kaur, Dinesh Singh Rana, *J. Mater. Sci. Mater. Electron.* **30**, 18153 (2019).
- [28] J. Yuh, J. C. Nino, W. Sigmund, *Mater. Lett.* **59**, 3645 (2005).
- [29] V. Vinothini, P. Singh, M. Balasubramanian, *Ceram. Int.* **32**, 99 (2006).
- [30] N. Joseph, S. K. Singh, R. K. Sirugudu, *Materials Research Bulletin* **48**, 1681 (2013).
- [31] Z. M. Dang, H. Y. Wang, Y. H. Zhang, *Macromol. Rapid Commun.* **26**, 1185 (2005).
- [32] Y. Qi, L. Pan, Li Ma, *Journal of Material Science Materials in Electronics* **24**, 1446 (2013).
- [33] Chandan Kumar, P. Viswanath, *J. of Applied Polymer Sci.* **136**, 47818(1) (2019).
- [34] H. Paranguan, D. Ponnamma, D. Al Ali Al Maadeed, *M. RSC Adv.* **7**, 50156 (2017).
- [35] N. J. Ramer, T. Marrone, K. Stiso, *J. Polym.* **47**, 7160 (2006).
- [36] S. Lanceros-Mendez, J. F. Mano, A. M. Costa, V. H. Schmidt, *J. Macromol. Sci. Physics* **B-40**, 517 (2001).
- [37] Dinesh Singh Rana, D. K. Chaturvedi, J. K. Quamara, *Proc. I. Mech. Engineers Part J- J. Engineering Tribology* **224**, 667 (2010).
- [38] X. Cai, T. Lei, D. Sun, *RSC Adv.* **7**, 15382 (2017).
- [39] Hoejin Kim, F. Torres, Dino Villagran, *Macromol. Mater. Eng.* **302**, 1700229(1) (2017).

*Corresponding author: gurpreet92engg@gmail.com,
rana.kuk@gmail.com